2011 50th IEEE Conference on Decision and Control and
European Control Conference (CDC-ECC)
Orlando, FL, USA, December 12-15, 2011

An Adaptive Energy-Efficient Control Allocation on Planar Motion Control of Electric Ground Vehicles

Yan Chen and Junmin Wang*
Department of Mechanical and Aerospace Engineering
The Ohio State University
Columbus, OH 43210

Abstract—**An adaptive energy-efficient control allocation (A-EECA) is developed for planar motion control of electric ground vehicles (EGVs) with four in-wheel motors. Different from distribution processes in previous EECA designs [19][28], which needed to instantaneously solve nonlinear (even non-convex) optimization problems at each sampling time, this adaptive EECA approach can make distributed control actuation gradually converge to energy-optimal operating points. The consequent advantages are reflected in both low computational cost and free selections of initial conditions. Based on experimental data and some reasonable assumptions on the efficiencies of in-wheel motors, the adaptive EECA dictates different torque distributions to all the EGV wheels based on their different efficiencies. Simulation results of different maneuvers indicate that much less energy and computational cost are consumed when the adaptive EECA scheme is applied for controlling the planar motion of an EGV.**

I. Introduction

ELECTRIC ground vehicles (EGVs) have attracted increasing attention from both industrial and academic communities recently. On one hand, electrical machines and energy management technologies involved in hybrid electrical vehicles (HEVs) and plug-in hybrid electrical vehicles (PHEVs) have become mature, which could be heuristically applied to EGVs. On the other hand, high energy-density and power-density batteries and in-wheel motors with fast and accurate torque control capabilities offer other opportunities for the development of pure EGVs with four independently actuated in-wheel motors [1]-[4].

In conventional vehicle powertrain architectures, even for HEVs and PHEVs, driving and braking actions of different wheels are coupled by mechanical transmissions and/or differentials. Comparably, EGVs with independently actuated (driving and regenerative braking) in-wheel motors can provide a unique advantage of higher control flexibility [20][30][31] and other consequent potentials, such as real-time tire-road friction coefficient estimation independent of vehicle longitudinal motion [5]. However, this unique configuration also brings a more challenging problem of control because an EGV with four independently-actuated in-wheel motors is an over-actuated system, where the number of actuators is greater than the system degrees of freedom [6][7]. For over-actuated systems, control allocation (CA) is a common approach to distribute desired virtual controls to all the available actuators within their respective constraints [3][4]. Many CA algorithms, which were usually formulated as numerical optimization problems, were applied to ground vehicles. Plumlee *et al.* [11] applied CA to a linearized vehicle model in order to track a desired yaw rate trajectory, which was solved based on quadratic programming (QP). Wang *et al.* [4] improved a QP-based CA algorithm for coordinated vehicle dynamic control by considering vehicle operating condition and tire-road friction. Moreover, Tagesson *et al.* [12] compared two numerical CA algorithms, active-set and primal-dual interior point, for the real-time performance when they were applied to the yaw motion control of heavy vehicles. The aforementioned CA applications on vehicles all solve optimal CA problems at instantaneous time, which however require considerably high computational costs.

Given virtual control information offline, Gerard and Verhaegen [13][14] suggested that tire force distributions in a two-layer chassis control law were not necessarily optimized at each time step, but trended in the optimal direction for a convex CA problem. Tjønnås and Johansen [15][16] developed a general adaptive CA algorithm that largely save computational cost based on a Lyapunov method, with applications on brake control to achieve yaw stabilization of a vehicle for extreme maneuvers. Liao *et al.* [8][18] extended the adaptive CA work to nonlinear systems with internal dynamics with applications on a non-minimum phase aircraft system.

Within the aforementioned vehicle applications, the adopted CA algorithms, adaptive or non-adaptive, rarely considered energy optimization during virtual control distributions, though different vehicle performances were achieved. Since minimum actuation magnitudes for actuators do not necessarily lead to minimum power consumption due to actuators' efficiency characteristics, the authors [19][28] proposed an energy-efficient control allocation (EECA) scheme to simultaneously achieve energy optimization as well as desired vehicle dynamics control. However, previous EECA methods [28] needed to instantaneously solve complex non-convex optimization problems to distribute torques, which is challenging to be implemented due to limited computational capacities on EGVs. Based on the adaptive CA [16][17], the proposed adaptive EECA with a modified slack parameter, which is novelly introduced to guarantee equality conditions for working-mode selections of in-wheel motors, can make torque distributions gradually converge to energy-optimal operating points while maintaining EGV's

*Corresponding author. Yan Chen (e-mail: chen.1843@osu.edu) and Junmin Wang (e-mail: wang.1381@osu.edu). This research was supported by the Office of Naval Research Young Investigator Program (ONR-YIP) Award under Grant N00014-09-1-1018, Honda-OSU Partnership Program, and OSU Transportation Research Endowment Program.

planar motion control. It requires less computational cost and is more feasible for real vehicle implementations.

The remainder of this paper is organized as follows. In section II, a control-oriented model for vehicle planar motion and a higher-level sliding mode controller are reviewed. The adaptive EECA is developed in section III. In section IV, co-simulations with Simulink and CarSim are applied for different vehicle maneuvers in order to verify savings on both energy and computational cost of the adaptive EECA. Conclusive remarks are presented in section V.

II. VEHICLE MODEL AND HIGH-LEVEL CONTROLLER

For self-completeness, a control-oriented model for EGV planar motion and a higher-level sliding mode controller (SMC) are reviewed in this section. Descriptions in detail are referred to [28].

A. EGV control-oriented model for planar motion

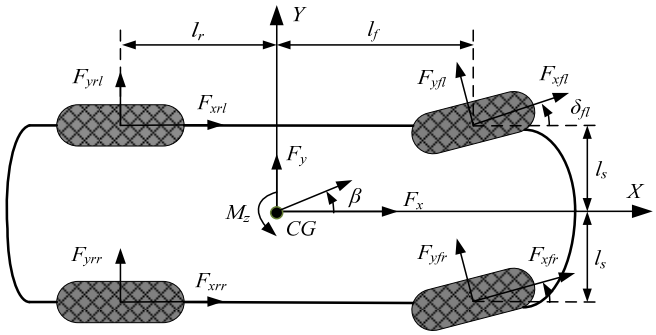

Figure 1. Coordinates for planar motions of EGV.

Figure 1 displays the EGV planar motion coordinates (longitudinal, lateral, and yaw). Let $x_1 = v_x$, $x_2 = v_y$ and $x_3 = r$, a nonlinear control-oriented model is obtained as follows [28].

$$\begin{aligned}
\dot{x}_1 &= x_2 x_3 - \frac{C_a}{m_v} x_1^2 + \frac{1}{m_v}\left(\frac{-J}{R_{eff}} \Delta_{1x} \dot{\omega} + \Delta_{1y} F_Y \right) + v_1 \\
\dot{x}_2 &= -x_1 x_3 + \frac{1}{m_v}\left(\frac{-J}{R_{eff}} \Delta_{2x} \dot{\omega} + \Delta_{2y} F_Y \right) + v_2 \\
\dot{x}_3 &= \frac{1}{I_z}\left(\frac{-J}{R_{eff}} \Delta_{3x} \dot{\omega} + \Delta_{3y} F_Y \right) + v_3
\end{aligned} \quad , \tag{1}$$

where

$$F_Y = \begin{bmatrix} F_{yfl} & F_{yfr} & F_{yrl} & F_{yrr} \end{bmatrix}^T, \dot{\omega} = \begin{bmatrix} \dot{\omega}_{fl} & \dot{\omega}_{fr} & \dot{\omega}_{rl} & \dot{\omega}_{rr} \end{bmatrix}^T$$

$$\Delta_{1x} = \begin{bmatrix} \cos\delta_{fl} & \cos\delta_{fr} & 1 & 1 \end{bmatrix}, \Delta_{1y} = \begin{bmatrix} -\sin\delta_{fl} & -\sin\delta_{fr} & 0 & 0 \end{bmatrix},$$

$$\Delta_{2x} = \begin{bmatrix} \sin\delta_{fl} & \sin\delta_{fr} & 0 & 0 \end{bmatrix}, \Delta_{2y} = \begin{bmatrix} \cos\delta_{fl} & \cos\delta_{fr} & 1 & 1 \end{bmatrix},$$

$$\Delta_{3x} = \begin{bmatrix} l_f \sin\delta_{fl} - l_s \cos\delta_{fl} & l_s \cos\delta_{fr} + l_f \sin\delta_{fr} & -l_s & l_s \end{bmatrix},$$

$$\Delta_{3y} = \begin{bmatrix} l_s \sin\delta_{fl} + l_f \cos\delta_{fl} & l_f \cos\delta_{fr} - l_s \sin\delta_{fr} & -l_r & -l_r \end{bmatrix}.$$

Moreover, the virtual control v_d is expressed as

$$v_d = \begin{bmatrix} v_1 & v_2 & v_3 \end{bmatrix}^T = Bu \ , \tag{2}$$

with

$$B = \begin{bmatrix} \Delta_{1x}^T / m_v R_{eff} & \Delta_{2x}^T / m_v R_{eff} & \Delta_{3x}^T / I_z R_{eff} \end{bmatrix}^T ,$$

$$u = \begin{bmatrix} T_1 & T_2 & T_3 & T_4 \end{bmatrix}^T .$$

B. Higher-level sliding mode control

In order to track the desired planar motions, a hierarchical control strategy consisting of a higher-level SMC and a lower-level adaptive EECA algorithm is adopted. The SMC offers the generalized forces/moments (virtual control) required to track the desired vehicle planar motions and accommodates uncertainties involved in vehicle dynamics.

For the control-oriented model (1), the SMC design is partitioned into three single-input-single-output systems since the virtual control inputs are decoupled. Furthermore, by considering a potential problem of yaw rate error accumulation due to chattering effects of SMC design, the modified three virtual control signals are directly displayed in the following [28].

$$v_1 = -x_2 x_3 + \frac{C_a}{m_v} x_1^2 - \frac{1}{m_v}\left(\frac{-J}{R_{eff}} \Delta_{1x} \dot{\omega} + \Delta_{1y} \hat{F}_Y \right) + \dot{x}_{1r} - k_1 \mathrm{sat}(s_1) \tag{3}$$

$$v_2 = x_1 x_3 - \frac{1}{m_v}\left(\frac{-J}{R_{eff}} \Delta_{2x} \dot{\omega} + \Delta_{2y} \hat{F}_Y \right) + \dot{x}_{2r} - k_2 \mathrm{sat}(s_2) \tag{4}$$

$$v_3 = -\frac{1}{I_z}\left(\frac{-J}{R_{eff}} \Delta_{3x} \dot{\omega} + \Delta_{3y} \hat{F}_Y \right) + \dot{x}_{3r} - k_3 \mathrm{sat}(s_3) \tag{5}$$

where the sliding surfaces are denoted by $s_m \ (m = 1,2,3)$. Within the above equations, the control gain $k_m > 0$ can be appropriately selected to address the parameter uncertainties. x_{mr} represents the reference longitudinal, lateral speed, and yaw rate, respectively. The estimated lateral friction force $\hat{F}_Y$ is calculated based on a Magic Formula tire model [22], which is generally accepted as a fairly accurate model and widely adopted in vehicle dynamical simulations and analyses [23][24][27]. Angular acceleration $\dot{\omega}$ can be estimated through Kalman filters for noisy angular velocities measured from four independent wheel-speed sensors. Saturation function $\mathrm{sat}(\cdot)$ instead of $\mathrm{sign}(\cdot)$ function is applied to reduce chattering effects in practical implementation of the control laws [25][26]. Thus, the control laws shown in (3), (4) and (5) ensure the EGV planar motion tracking.

III. ADAPTIVE EECA DESIGN

Based on the virtual control expression (2), the EECA problem is formulated as follow,

$$\min J_e = \frac{1}{2}\left(B_a \begin{bmatrix} u & u' \end{bmatrix} - v_d\right)^T W_v \left(B_a \begin{bmatrix} u & u' \end{bmatrix} - v_d\right) + \sigma P_c$$

$$\text{s.t.} \begin{cases} u_{\min} \le u \le u_{\max} \\ u'_{\min} \le u' \le u'_{\max} \\ (u_i - \varepsilon)(u'_i + \varepsilon) = 0, i = 1, \ldots, 4 \end{cases} , \tag{6}$$

where the virtual actuators $u' = \begin{bmatrix} T_1' & T_2' & T_3' & T_4' \end{bmatrix}^T$ are introduced to represent in-wheel motor regenerative braking torques. The control effectiveness matrix is represented as

$B_a = [B \quad B]$. W_v and σ are a positive definite weighting matrix and a weighting factor, respectively. The above constraints apply to the real and virtual actuators component-wisely. The introduction of virtual actuators and the division of control effect into driving/braking cases (u/u') are due to their different power consumptions and efficiencies [19][30]. Compared with the EECA formulation in [20][28], the equality constraints in (6), which ensure that only one operating mode is assigned to an actuator at any given time instant, are all modified with a small constant slack number $\varepsilon > 0$ for developing the adaptive control law shown as follows.

Within (6), the total power consumption of four in-wheel motors for dual operating modes is formulated as

$$P_c = \sum_{i=1}^{4} \frac{P_{oi}(u_i)}{\eta_{oi}(u_i)} - \sum_{i=1}^{4} P_{ii}(u'_i)\eta_{ii}(u'_i). \tag{7}$$

Here, P_{oi} denotes the output power at the energy consuming mode and P_{ii} is the input power at the energy gaining mode. The actuator efficiencies at energy consuming and gaining modes are represented by η_{oi} and η_{ii}, respectively. The energy gaining mode is inferred by the minus sign in (7). Before the main result is shown, two preliminary definitions are introduced first.

Define the corresponding Lagrangian function for (6) as,

$$\begin{aligned} &L\left(v_d(x,x_r),\delta,u,u',\lambda\right) \\ &= \frac{1}{2}\left(B_a[u \quad u']^T - v_d\right)^T W_v \left(B_a[u \quad u']^T - v_d\right) \\ &+\sigma\left(\sum_{i=1}^{4}\frac{P_{oi}(u_i)}{\eta_{oi}(u_i)} - \sum_{i=1}^{4} P_{ii}(u'_i)\eta_{ii}(u'_i)\right) \\ &+\sum_{i=1}^{4}\lambda_i(u_i-\varepsilon)(u'_i+\varepsilon) + \mu\sum_{i,j=1}^{4}\log C_{ij}(u,u') \end{aligned} \tag{8}$$

where $C_{1j}(u,u') = u_j - (u_{\min})_j$, $C_{2j}(u,u') = (u_{\max})_j - u_j$, $C_{3j}(u,u') = u'_j - (u'_{\min})_j$ and $C_{4j}(u,u') = (u'_{\max})_j - u'_j$ $(j = 1,\cdots,4)$. $\lambda = [\lambda_1 \quad \lambda_2 \quad \lambda_3 \quad \lambda_4]^T$ is the vector of Lagrangian multipliers. $\mu > 0$ is a constant for logarithm barrier functions. The two front tire steering angles δ_{fl} and δ_{fr} are equal to the steering angle δ because of the small ratio between the vehicle track and wheelbase.

Since local minima of (8) satisfy the first-order optimality conditions [21], an optimal set E^* is defined as

$$E^* = \left\{(u,u',\lambda) \mid \frac{\partial L}{\partial u} = 0, \frac{\partial L}{\partial u'} = 0, \frac{\partial L}{\partial \lambda} = 0\right\}. \tag{9}$$

Note that $\partial L/\partial\lambda = 0$ in the definition of E^* guarantees equality constraints in (6). When the optimal set is reached, $u_i = \varepsilon$ (or $u'_i = -\varepsilon$) is compatible with the other two optimal conditions $\partial L/\partial u = 0$ and $\partial L/\partial u' = 0$. If the slack number is not adopted, $u_i = 0$ (or $u'_i = 0$) will make the $\partial L/\partial u$ (or $\partial L/\partial u'$) go to infinity due to the derivatives of the logarithm barrier functions with common boundary values $u_{\min} = u'_{\max} = 0$. The relationship between the original nonlinear optimization problem (6)-(7) and the two preceding definitions is shown through the following lemma.

Lemma 1 The problem (6)-(7) achieves local minima if and only if the optimal set E^* is reached.

***Proof*:** The necessity is obvious based on the first necessary optimal condition [21]. The sufficiency can be obtained by observing the second derivatives $\partial^2 L/\partial u^2 > 0$ and $\partial^2 L/\partial u'^2 > 0$ from the expressions shown in the Appendix. According to the perturbation theory for real symmetric matrices [29], the bounded power and boundary related terms can be all dominated by the positive definite matrix $B^T W_v B$ by suitably selecting certain small positive numbers σ and μ. Thus, the sufficiency is guaranteed by the second-order sufficient condition [21]. ■

Theorem 1 $\{u,u',\lambda\} \to E^*$ as $t \to \infty$ when the following update laws for control inputs and Lagrangian multipliers are adopted:

$$\begin{aligned} \dot{u} &= -\Gamma_1\alpha + \varphi_1 \\ \dot{u}' &= -\Gamma_2\beta + \varphi_2, \\ \dot{\lambda} &= -\Gamma_3\gamma + \varphi_3 \end{aligned} \tag{10}$$

where $\Gamma_1 = \Gamma_1^T > 0$, $\Gamma_2 = \Gamma_2^T > 0$, and $\Gamma_3 = \Gamma_3^T > 0$ are constant matrices. Vectors α, β, and γ are defined as

$$\begin{pmatrix}\alpha\\ \beta\\ \gamma\end{pmatrix} = \begin{bmatrix} \frac{\partial^2 L}{\partial u^2} & \left(\frac{\partial^2 L}{\partial u'\partial u}\right)^T & \left(\frac{\partial^2 L}{\partial\lambda\partial u}\right)^T \\ \left(\frac{\partial^2 L}{\partial u\partial u'}\right)^T & \frac{\partial^2 L}{\partial u'^2} & \left(\frac{\partial^2 L}{\partial\lambda\partial u'}\right)^T \\ \left(\frac{\partial^2 L}{\partial u\partial\lambda}\right)^T & \left(\frac{\partial^2 L}{\partial u'\partial\lambda}\right)^T & 0 \end{bmatrix} \begin{pmatrix}\frac{\partial L}{\partial u}\\ \frac{\partial L}{\partial u'}\\ \frac{\partial L}{\partial\lambda}\end{pmatrix} = H\begin{pmatrix}\frac{\partial L}{\partial u}\\ \frac{\partial L}{\partial u'}\\ \frac{\partial L}{\partial\lambda}\end{pmatrix} \tag{11}$$

and φ_1, φ_2, and φ_3 are vectors satisfying the following scalar time-varying algebraic equation

$$\alpha^T\varphi_1 + \beta^T\varphi_2 + \gamma^T\varphi_3 + \tau = 0. \tag{12}$$

where τ is defined as

$$\begin{aligned} \tau &= \left(\frac{\partial L^T}{\partial u}\frac{\partial^2 L}{\partial u\partial v_d} + \frac{\partial L^T}{\partial u'}\frac{\partial^2 L}{\partial u'\partial v_d}\right)\dot{v}_d \\ &+\left(\frac{\partial L^T}{\partial u}\frac{\partial^2 L}{\partial u\partial\delta} + \frac{\partial L^T}{\partial u'}\frac{\partial^2 L}{\partial u'\partial\delta}\right)\dot{\delta} \end{aligned} \tag{13}$$

***Proof*:** A control Lyapunov function candidate is defined as

$$V\left(x,v_d,\delta,u,u',\lambda\right) = \frac{1}{2}\left(\frac{\partial L^T}{\partial u}\frac{\partial L}{\partial u} + \frac{\partial L^T}{\partial u'}\frac{\partial L}{\partial u'} + \frac{\partial L^T}{\partial\lambda}\frac{\partial L}{\partial\lambda}\right) \tag{14}$$

The derivative of V along the nonlinear system (1) gives,

$$\begin{aligned} &\dot{V}\left(v_d(x,x_r),\delta,u,u',\lambda_i\right) \\ &= \frac{\partial L^T}{\partial u}\frac{\partial}{\partial t}\left(\frac{\partial L}{\partial u}\right) + \frac{\partial L^T}{\partial u'}\frac{\partial}{\partial t}\left(\frac{\partial L}{\partial u'}\right) + \frac{\partial L^T}{\partial\lambda}\frac{\partial}{\partial t}\left(\frac{\partial L}{\partial\lambda}\right) \end{aligned}$$

$$
\begin{aligned}
&=\left(\frac{\partial L^T}{\partial u}\frac{\partial^2 L}{\partial u^2}+\frac{\partial L^T}{\partial u'}\frac{\partial^2 L}{\partial u'\partial u}+\frac{\partial L^T}{\partial \lambda}\frac{\partial^2 L}{\partial \lambda\partial u}\right)\dot{u}\\
&+\left(\frac{\partial L^T}{\partial u}\frac{\partial^2 L}{\partial u\partial u'}+\frac{\partial L^T}{\partial u'}\frac{\partial^2 L}{\partial u'^2}+\frac{\partial L^T}{\partial \lambda}\frac{\partial^2 L}{\partial \lambda\partial u'}\right)\dot{u}'\\
&+\left(\frac{\partial L^T}{\partial u}\frac{\partial^2 L}{\partial u\partial \lambda}+\frac{\partial L^T}{\partial u'}\frac{\partial^2 L}{\partial u'\partial \lambda}\right)\dot{\lambda}+\left(\frac{\partial L^T}{\partial u}\frac{\partial^2 L}{\partial u\partial v_d}+\frac{\partial L^T}{\partial u'}\frac{\partial^2 L}{\partial u'\partial v_d}\right)\dot{v}_d\\
&+\left(\frac{\partial L^T}{\partial u}\frac{\partial^2 L}{\partial u\partial \delta}+\frac{\partial L^T}{\partial u'}\frac{\partial^2 L}{\partial u'\partial \delta}\right)\dot{\delta}.
\end{aligned}
\tag{15}
$$

From the expressions of α^T, β^T, γ^T and τ in (11) and (13), $\dot{V}$ in (15) is rewritten as

$$\dot{V}\left(x,v_d,\delta,u,u',\lambda_i\right)=\alpha^T\dot{u}+\beta^T\dot{u}'+\gamma^T\dot{\lambda}+\tau.$$

Substituting (10) and (12) in,

$$\dot{V}\left(x,v_d,\delta,u,u',\lambda_i\right)=-\alpha^T\Gamma_1\alpha-\beta^T\Gamma_2\beta-\gamma^T\Gamma_3\gamma$$

the proof is completed by showing the H matrix is non-singular, which guarantees the equivalence between α,β,γ and $\partial L/\partial u,\partial L/\partial u',\partial L/\partial\lambda$. Based on the expressions shown in Appendix, the determinant of H is represented as

$$
\begin{aligned}
\det(H)&=\det\begin{pmatrix}
-\frac{\partial^2 L}{\partial u'\partial\lambda}\left(\frac{\partial^2 L}{\partial u^2}\frac{\partial^2 L}{\partial u'\partial\lambda}-\frac{\partial^2 L}{\partial u\partial u'}\frac{\partial^2 L}{\partial u\partial\lambda}\right)\\
+\frac{\partial^2 L}{\partial u\partial\lambda}\left(\frac{\partial^2 L}{\partial u\partial u'}\frac{\partial^2 L}{\partial u'\partial\lambda}-\frac{\partial^2 L}{\partial u'^2}\frac{\partial^2 L}{\partial u\partial\lambda}\right)
\end{pmatrix}\\
&=\det\begin{pmatrix}
-\mathrm{diag}^2\left(u-\varepsilon I_{4\times1}\right)\frac{\partial^2 L}{\partial u^2}\\
+2\mathrm{diag}\left[\left(u-\varepsilon I_{4\times1}\right)\left(u'+\varepsilon I_{4\times1}\right)\right]\left(B^TW_vB+\mathrm{diag}\left(\lambda\right)\right)\\
-\mathrm{diag}^2\left(u'+\varepsilon I_{4\times1}\right)\frac{\partial^2 L}{\partial u'^2}
\end{pmatrix}.
\end{aligned}
$$

Since $\partial^2L/\partial u^2>0$, $\partial^2L/\partial u'^2>0$ (as shown in Lemma 1 proof) and $B^TW_vB>0$, nonzero determinant of matrix H is guaranteed because $u-\varepsilon I_{4\times1}$ and $u'+\varepsilon I_{4\times1}$ cannot be zeros simultaneously when $v_d\neq0$. ■

***Remarks*:** Following Lemma 2 in [17], one common approach to make the scalar time-varying algebraic equation (12) always hold is to solve the corresponding least-square problem. Define a new Lagrangian function with a Lagrangian multiplier λ_{L_1},

$$
\begin{aligned}
L_1\left(\varphi_1,\varphi_2,\varphi_3,\lambda_{L_1}\right)&=\frac{1}{2}\left(\varphi_1^T\varphi_1+\varphi_2^T\varphi_2+\varphi_3^T\varphi_3\right)\\
&+\lambda_{L_1}\left(\alpha^T\varphi_1+\beta^T\varphi_2+\gamma^T\varphi_3+\tau\right)
\end{aligned}
\tag{16}
$$

Through the first-order optimality conditions $\partial L_1/\partial\varphi_m=0$ and $\partial L_1/\partial\lambda_{L_1}=0$, the following linear equations are obtained

$$
\begin{bmatrix}
I & 0 & 0 & \alpha\\
0 & I & 0 & \beta\\
0 & 0 & I & \gamma\\
\alpha^T & \beta^T & \gamma^T & 0
\end{bmatrix}
\begin{bmatrix}
\varphi_1\\ \varphi_2\\ \varphi_3\\ \lambda_{L_1}
\end{bmatrix}=
\begin{bmatrix}
0\\ 0\\ 0\\ -\tau
\end{bmatrix}.
\tag{17}
$$

Thus, when α, β and γ are not all zeros, equation (17) and consequently (12) has a unique solution. In the case of $\alpha=\beta=\gamma=0$, the trivial solutions are defined by $\varphi_1=\varphi_2=\varphi_3=0$.

IV. Simulation Results and Discussions

In this section, different maneuvers are simulated to verify the effectiveness of the adaptive EECA algorithms. The power consumptions, computational cost, and torque distributions are compared with those of standard CA methods, in which the magnitude of control were often minimized during CA process [3][8][13][18].

The experimental data for driving and regenerative braking efficiencies of in-wheel motors are first described as follows.

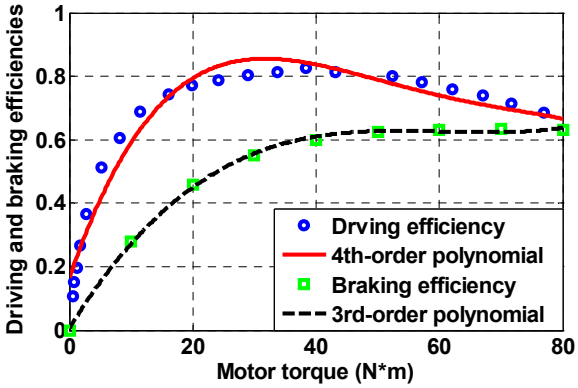

Figure 2. Driving and regenerative braking efficiency curve fitting of an in-wheel BLDC motor based on experimental data.

As shown in Figure 2, the driving and regenerative braking efficiencies of one in-wheel motor, $\eta_d(T)$ and $\eta_b(T')$, are expressed by fitting two groups of a BLDC in-wheel motor experimental data at a constant rotational speed.

$$
\begin{aligned}
\eta_d(T)&=p_1T^4+p_2T^3+p_3T^2+p_4T+p_5\\
\eta_b(T')&=p'_1T'^3+p'_2T'^2+p'_3T'+p'_4
\end{aligned}
\tag{18}
$$

Constant coefficients are represented by p_l, $l=1,\cdots,5$ and p'_j. Note that although the motor speed may also affect the motor efficiency, the efficiency curves are similar within a large range of motor rotational speeds based on experimental tests [28]. Moreover, the regenerative braking efficiency curve is always lower than the driving efficiency, which is reasonable for a real in-wheel motor and more experimental data can be found in [30].

Table 1 Simulation Parameters

Symbol	Values	Symbol	Values
p_1	-7.2888e-5	m_v	800 kg
p_2	1.8023e-5	I_z	729
p_3	-0.0016099	σ	1e-3
p_4	0.057038	R_{eff}	0.312 m
p_5	0.16446	J	1.4
p'_1	3.5227e-6	C_a	0.37
p'_2	-0.00061109	l_f	0.85 m
p'_3	0.034213	l_s	0.7 m
p'_4	0.010455	l_r	1.04 m
ε	0.5	μ	1e-5
$u'_{\min}$	-80 Nm	$u_{\max}$	80 Nm

All the simulation parameters are displayed in Table 1. Moreover, different working conditions/health status will make the four in-wheel motors' efficiencies different besides the manufacturing processes. Although the differences may not be huge under normal operations, four identical efficiencies in-wheel motors cannot be assumed. Without loss of generality, both driving and regenerative braking efficiencies of two rear in-wheel motors are scaled by 0.8 respectively to conveniently explain the simulation results.

The power functions P_{oi} (P_{ii}) in (7) are written as

$$P_{oi} = T_i\omega_i; P_{ii} = T_i\omega_i, \quad (19)$$

where the rotational wheel speeds can be measured through four independent wheel speed sensors.

A combined maneuver of the EGV first contains an acceleration process from 20 km/h to 30 km/h within 10 seconds. Then a single lane change (SLC) is commanded at a constant speed from the 20th second to the 30th second. Finally, the vehicle speed is decelerated to 20 km/h from the 40th second to the 50th second. The control results and torque distributions by using the adaptive EECA are shown in Figure 3 and Figure 4, respectively.

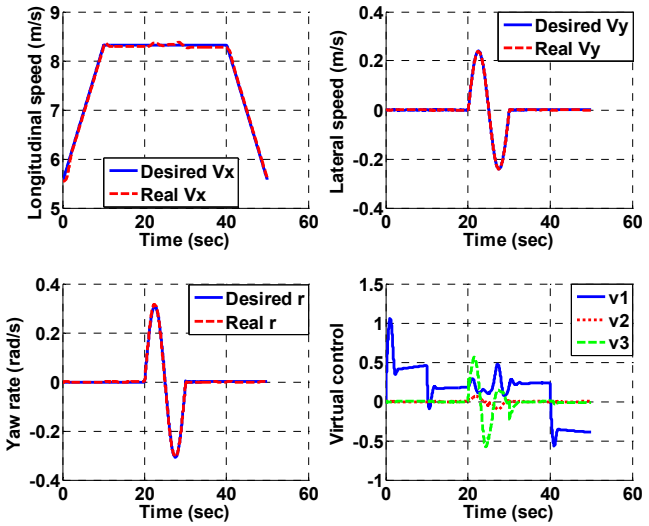

Figure 3. Tracking control effect of planar motion and virtual control for the adaptive EECA.

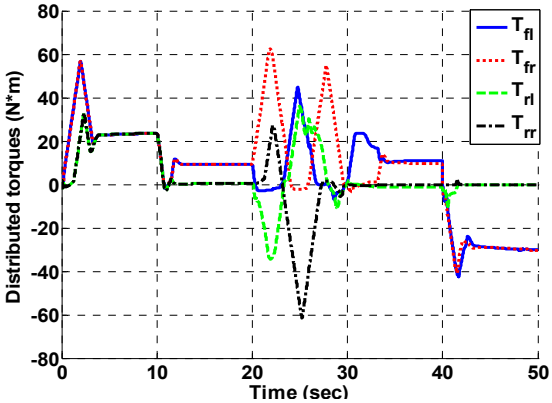

Figure 4. Torque distributions under the adaptive EECA scheme.

From Figure 3, the desired longitudinal, lateral speed and yaw rate are tracked well under the high-level SMC. The virtual controls generated by the SMC are distributed to four in-wheel motors by the adaptive EECA to optimize the total power consumptions (7). As shown in Figure 4, during the acceleration period, two front high-efficiency motors exert larger driving torques than two rear low-efficiency motors to reduce overall power consumptions. Note that a transient process is shown before reaching a steady state distribution. In the deceleration period, two front motors also absorb higher power by exerting larger regenerative braking torques than two rear motors. During the SLC maneuver, the high-efficiency front motors are always distributed with larger driving torques than the low-efficiency rear motors for optimal power consumptions.

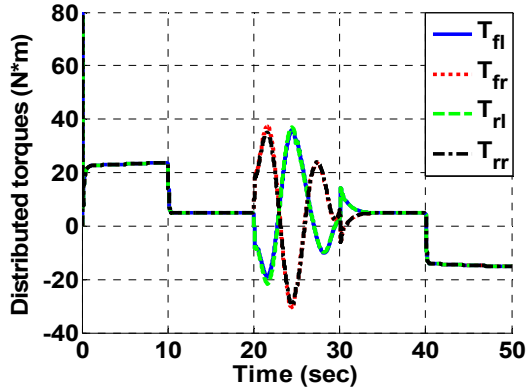

Figure 5. Torque distributions under the standard CA algorithm.

Although the standard CA algorithm can also give good tracking results, similar to the results shown in Figure 3, the driving/braking torques are just equally distributed to the four or two motors according to the motion requirements, as shown in Figure 5. This torque distribution scheme, which does not consider different efficiencies of actuators, cannot guarantee optimal power consumption during EGV planar maneuvers. Figure 6 illustrates this point.

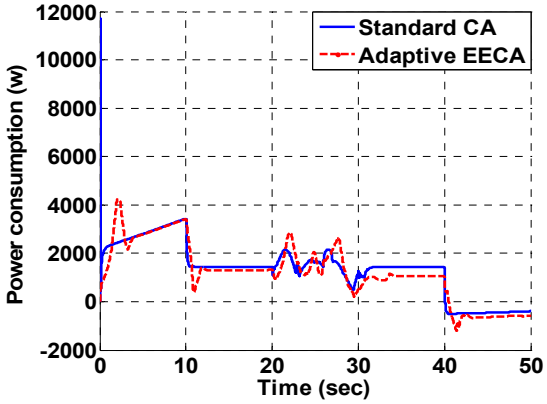

Figure 6. Power consumption comparison between the standard CA and the adaptive EECA.

Figure 6 shows instantaneous power consumptions for both the standard CA and the adaptive EECA during the 50 seconds. By integrating the instantaneous power consumptions along time for the 50 seconds, the total energy consumes in the standard CA procedure is 67.15 kJ, which is larger than that consumed in the adaptive EECA case, 61.76 kJ by 9%. It is clear that the adaptive EECA consumes less

power at the most time period. It is expected that the energy saving will accumulatively increase and become considerable as the travel time is prolonged. Moreover, under the same simulation conditions, the computational time for the adaptive EECA is about 50 seconds, while the time for the standard CA is about 36 minutes, which is about 40 times slower than the adaptive EECA.

APPENDIX

$$\left(\frac{\partial^2 L}{\partial u^2}\right)_{4\times 4} = B^T W_v B + \sigma \operatorname{diag}\left[\frac{\partial}{\partial u}\left(\frac{\frac{\partial P_o(u)}{\partial u}\eta_o(u) - P_o(u)\frac{\partial \eta_o(u)}{\partial u}}{\eta_o^2(u)}\right)\right]$$

$$+\mu \operatorname{diag}\left[\frac{1}{\left(u-u_{\min}\right)^2} + \frac{1}{\left(u_{\max}-u\right)^2}\right]$$

$$\left(\frac{\partial^2 L}{\partial u'^2}\right)_{4\times 4} = B^T W_v B - \sigma\left[\begin{array}{l}\operatorname{diag}\left(\frac{\partial^2 P_i(u')}{\partial u'^2}\eta_i(u') + \frac{\partial P_i(u')}{\partial u'}\frac{\partial \eta_i(u')}{\partial u'}\right) \\ +\operatorname{diag}\left(\frac{\partial^2 \eta_i(u')}{\partial u'^2}P_i(u') + \frac{\partial P_i(u')}{\partial u'}\frac{\partial \eta_i(u')}{\partial u'}\right)\end{array}\right]$$

$$+\mu \operatorname{diag}\left[\frac{1}{\left(u'-u'_{\min}\right)^2} + \frac{1}{\left(u'_{\max}-u'\right)^2}\right]$$

$$\left(\frac{\partial^2 L}{\partial u \partial u'}\right)_{4\times 4} = \left(\frac{\partial^2 L}{\partial u' \partial u}\right)_{4\times 4} = B^T W_v B + \operatorname{diag}(\lambda)$$

$$\left(\frac{\partial^2 L}{\partial u \partial \lambda}\right)_{4\times 4} = \left(\frac{\partial^2 L}{\partial \lambda \partial u}\right)_{4\times 4} = \operatorname{diag}\left(u' + \varepsilon I_{4\times 1}\right)$$

$$\left(\frac{\partial^2 L}{\partial u' \partial \lambda}\right)_{4\times 4} = \left(\frac{\partial^2 L}{\partial \lambda \partial u'}\right)_{4\times 4} = \operatorname{diag}\left(u - \varepsilon I_{4\times 1}\right)$$

V. CONCLUSIONS AND FUTURE WORK

This paper proposes an adaptive EECA for planar motion control of an EGV, actuated by four independently in-wheel motors. Different maneuvers are tested for the comparison of power consumption, computational cost, and torque distribution between the standard and the adaptive EECA. In order to asymptotically optimize power consumptions during planar motion maneuvers, the EECA dictates different torque distributions on in-wheel motors with different efficiencies compared with the standard CA method. Thus, less energy and computational cost are consumed when the adaptive EECA is applied. The future work includes experimental validation and robustness analyses of the control algorithms.

REFERENCES

[1] S. J. Hallowell and L. R. Ray, "All-wheel driving using independent torque control of each wheel," *Proceedings of the 2003 American Control Conference*, pp. 2590 – 2595, 2003.

[2] G. S. Buja and M. P. Kazmierkowski, "Direct torque control of PWM inverter-fed AC motors-a survey," *IEEE Transactions on Industrial Electronics*, Vol. 51, No. 4, pp. 744 –757, 2004.

[3] J. Wang and R. G. Longoria, "Coordinated and reconfigurable vehicle dynamics control," *IEEE Transactions on Control Systems Technology*, vol. 17, No. 3, pp. 723 – 732, 2009.

[4] J. Wang, J. M. Solis and R. G. Longoria, "On the control allocation for coordinated ground vehicle dynamics control systems," *Proceedings of the 2007 American Control Conference*, pp. 5724-5729, July, 2007.

[5] Y. Chen and J. Wang, "Adaptive Vehicle Speed Control with Input Injections for Longitudinal Motion Independent Road Frictional Condition Estimation," *IEEE Transactions on Vehicular Technology*, Vol. 60, No. 3, pp. 839 - 848, 2011.

[6] M. Oppenheimer, D. Doman and M. Bolender, "Control allocation for over-actuated systems," *14th Mediterranean conference on control and automation*, 2006.

[7] T. Fossen and T. Johansen, "A survey of control allocation methods for ships and underwater vehicles," *14th Mediterranean conference on control and automation*, 2006.

[8] M. Benosman, F. Liao, K. Lum and J. L. Wang, "Nonlinear control allocation for non-minimum phase systems," *IEEE Transactions on Control Systems Technology*, Vol. 17, No.2, pp. 394-404, March, 2009.

[9] H. Alwi and C. Edwards, "Fault tolerant control using sliding modes with on-line control allocation," *Automatica*, 44, pp. 1859-1866, 2008.

[10] J. Zheng, W. Su and M. Fu, "Dual-stage actuator control design using a doubly coprime factorization approach," *IEEE/ASME Transactions on Mechatronics*, Vol. 15, No. 1, 2010.

[11] J. H. Plumlee, D. M. Bevly and A. S. Hodel, "Control of a ground vehicle using quadratic programming based control allocation techniques," *Proceedings of the 2004 American Control Conference*, pp. 4704-4709, Boston, 2004.

[12] K. Tagesson, P. Sundström, L. Laine and N. Dela, "Real-time performance of control allocation for actuator coordination in heavy vehicles," *IEEE Intelligent Vehicles Symposium,* pp: 685 – 690, 2009.

[13] M. Gerard and M. Verhaegen, "Global and local chassis control based on load sensing," *Proceedings of the 2009 American Control Conference*, pp. 677-682, June, 2009.

[14] M. Gerard, B. Schutter and M. Verhaegen, "A hybrid steepest descent method for constrained convex optimization," *Automatica*, Vol. 45, pp. 525-531, 2009.

[15] J. Tjønnås and T. A. Johansen, "Stabilization of automotive vehicles using active steering and adaptive brake control allocation," *IEEE Transactions on Control Systems Technology*, Vol. 18, No. 3, pp. 545-558, May, 2010.

[16] J. Tjønnås and T. A. Johansen, "Adaptive control allocation," *Automatica*, Vol. 44, pp. 2754-2765, 2008.

[17] T. A. Johansen, "Optimizing nonlinear control allocation," *Proceedings of IEEE Conference on Decision and Control*, pp. 3435-3440, 2004.

[18] F. Liao, K. Y. Lum, J. L. Wang, and M. Benosman, "Adaptive control allocation for non-linear systems with internal dynamics," *IET Control Theory and Applications*, Vol. 4, Iss. 6, pp. 909-922, 2010.

[19] Y. Chen and J. Wang, "Energy-efficient control allocation for over-actuated systems with electric vehicle applications," *Proceedings of the 2010 ASME Dynamic Systems and Control Conference*, Boston, 2010.

[20] Y. Chen and J. Wang, "Fast and global optimal energy-efficient control allocation with applications to over-actuated electric ground vehicles", *IEEE Transactions on Control System Technology*, (in press), 2011 (DOI: 10.1109/TCST.2011.2161989).

[21] J. Nocedal and S. Wright, "Numerical Optimization," Springer, 2006.

[22] H. B. Pacejka and E. Bakker, "Magic formula tyre model," *Vehicle System Dynamics*, Vol. 21, No. Suppl: Tyre Models for Vehicle Dynamics Analysis, pp. 1-18, 1993.

[23] J. Y. Wong, *Theory of Ground Vehicles*. New Jersey: John Wiley & Sons, 2008.

[24] R. Rajamani, *Vehicle Dynamics and Control*, Springer, 2006.

[25] J.-J. E. Slotine and W. Li, *Applied Nonlinear Control*. Prentice Hall, 1991.

[26] V. Utkin, J. Guldner and J. Shi, *Sliding Mode Control in Electro-Mechanical Systems*. CRC Press, 2nd edition. 2009.

[27] R. N. Jazar, *Vehicle Dynamics: Theory and Application*, Springer, 2009.

[28] Y. Chen and J. Wang, "Energy-efficient control allocation with applications on planar motion control of electric ground vehicles," *Proceedings of the American Control Conference*, pp.5300-5305, 2011.

[29] J. H. Wilkinson, *The algebraic eigenvalue problem*, Oxford, 1965.

[30] R. Wang, Y. Chen, D. Feng, X. Huang, and J. Wang, "Development and Performance Characterization of an Electric Ground Vehicle with Independently Actuated In-Wheel Motors," *Journal of Power Sources*, Vol. 196, Issue 8, pp. 3962-3971, 2011.

[31] Rongrong Wang and Junmin Wang, "Fault-Tolerant Control for Electric Ground Vehicles with Independently-Actuated In-Wheel Motors," *ASME Transactions Journal of Dynamic Systems, Measurement, and Control* (in press), 2011.